# Aqueous friction behavior of swollen hydrophilic poly(ethylene glycol)-based polyurethane coatings

**Document license:**
TAVERNE

**DOI:**
10.1007/s10853-020-05580-9

**Document status and date:**
Published: 01/03/2021

**Document Version:**
Publisher's PDF, also known as Version of Record (includes final page, issue and volume numbers)

**Please check the document version of this publication:**

• A submitted manuscript is the version of the article upon submission and before peer-review. There can be important differences between the submitted version and the official published version of record. People interested in the research are advised to contact the author for the final version of the publication, or visit the DOI to the publisher's website.
• The final author version and the galley proof are versions of the publication after peer review.
• The final published version features the final layout of the paper including the volume, issue and page numbers.

Link to publication

## Invited Viewpoint

# Aqueous friction behavior of swollen hydrophilic poly(ethylene glycol)-based polyurethane coatings

Peter T. M. Albers[1,4], Jozua Laven[1,2], Leendert G. J. van der Ven[1], Rolf A. T. M. van Benthem[1,3], Gijsbertus de With[1,2,*] , and A. Catarina C. Esteves[1,*]

[1] *Laboratory of Physical Chemistry, Department of Chemical Engineering and Chemistry, Eindhoven University of Technology, Eindhoven, The Netherlands*

[2] *Laboratory of Materials and Interface Chemistry, Department of Chemical Engineering and Chemistry, Eindhoven University of Technology, Eindhoven, The Netherlands*

[3] *DSM Materials Science Center, Netherlands, P.O. Box 18, 6160, MD, Geleen, The Netherlands*

[4] *Dutch Polymer Institute (DPI), P. O. Box 902, 5600 AX Eindhoven, The Netherlands*

## ABSTRACT

The macroscopic friction behavior of water-swollen cross-linked poly(ethylene glycol)-based polyurethane coatings (PEG-based PU coatings) with varying PEG precursor mass is measured against a glass counter surface. Experimental data such as the water uptake and the indentation modulus are used to calculate an accurate value for the molar mass between cross-links $M_c$, which, in turn, is used for the estimation of the actual coating mesh size $\xi$. The friction, swelling and indentation data obtained are used to successfully deduce an empirical model for the quantitative description of the aqueous friction behavior of these coatings depending on the mesh size of the coatings and the sliding velocity only.

## Introduction

Hydrophilic polymeric coatings are applied to substrates and devices to reduce protein adhesion and to minimize drag resistance and friction arising upon moving such a surface through an aqueous medium or against an immersed counter surface. Hereby, these coatings provide the substrate or device with lubricity [1, 2]. This lubricity is particularly important for bio-medical devices in dynamic contact with the human body, in order to increase the patient's comfort and to reduce the risk of device-associated infections due to tissue damage and protein adhesion [3–5].

The type of hydrophilic coating to coat bio-medical devices, such as catheters, is often a highly hydrated hydrogel coating, either covalently or non-covalently bonded to the substrate [1, 6]. A vast variety of hydrophilic polymers is available for the design of hydrogels [7, 8], of which the most commonly ones

---

Handling Editor: C. Barry Carter.

Address correspondence to E-mail: g.dewith@tue.nl; a.c.c.esteves@tue.nl

used are poly(vinylpyrrolidone) (PVP) [9–12], poly(-ethylene glycol) (PEG) [13–15], polysaccharides [16, 17] and co-polymers thereof [18–20]. These coatings are often applied via dip coating processes, with a subsequent polymerization step to graft the polymer layer to the substrate (or to a primer layer) or solely to increase the cross-link density of the polymer coating [1, 12, 13, 16]. Although it is known that highly hydrated hydrogel coatings exhibit lubricity in an aqueous environment due to the hydrophilic nature of the polymer network, the friction behavior of these coatings is rather complex and still poorly understood. In particular, knowledge on the relation between the polymer network structure and the resulting lubricity is still largely lacking.

Apart from the friction behavior of thin lubricious coatings, the description of the friction behavior of hydrogels in general is already challenging per se [21–23]. In 1998, Gong and Osada proposed a friction mechanism for hydrogels based on repulsion and attraction of polymer chains against a smooth counter surface [24]. In the case of repulsion between the gel and the counter surface, the friction force is governed by the lubricious properties of the hydrated water layer at the interface and should be proportional to the sliding velocity. In the case of attraction, however, the friction behavior of the hydrogel originates from two different contributions: (1) lubrication of the hydrated water layer of the network and (2) elastic deformation of polymer chains adsorbed to the counter surface (as sketched in Fig. 1). The latter contribution is similar to the adhesive friction of rubbers described by Schallamach [25] and is based on the adsorption life-time and re-adsorption time of polymer chains to a counter surface. Their model makes use of polymer scaling relations [26] for describing a gel as a collection of adjacent blobs (spheres) with a relaxation time which is related to their radius. Next to the development of a hydrogel friction model, Gong and coworkers studied, among others, the normal load dependency [27], the effect of the hydrophobicity [28] and roughness [29] of the counter surface, the effect of the preparation conditions [30], the effect of the addition of charged brushes and the use of interpenetrated networks [31] on the friction behavior of various hydrogels. Although the trends observed could be explained qualitatively, quantitative descriptions remain challenging.

The hydrogel friction model of Gong and Osada shows a dependency on the cross-link density of the
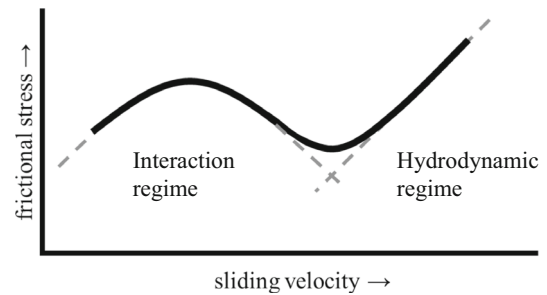


**Figure 1** Schematic of the friction curve for a gel with attractive interaction between gel and counter surface in a liquid as a function of sliding velocity as proposed by Gong and Osada [24] (adapted from Kurokawa et al. [23]).

hydrogels (via the modulus of elasticity $E$) at sliding velocities dominated by the elastic friction contribution [24]. This cross-link density dependency for the friction behavior of gels has also been shown by others [32, 33], and especially by Sawyer and coworkers for both hydrogel-hydrogel friction and hydrogel-solid friction [34–36]. For the former system, they report the existence of a so-called Gemini hydrogel interface for which the friction response at low velocities, in contrast to the adsorption-repulsion model, is independent of sliding speed or contact time [37, 38].

In order to increase the knowledge on the structure–friction relation of lubricious coatings, the aim of this work is to quantitatively relate the mesh size of water-swollen chemically cross-linked hydrophilic polymer coatings with the resulting macroscopic friction response against a rigid counter surface. Since a well-defined network architecture is required in such a study, the use of an end-linking step growth polymerization chemistry is preferred over free radical initiated chain growth polymerization chemistries [39, 40]. Next to the wide acceptance of PEG in the bio-medical field for its biocompatibility and anti-protein fouling properties [1, 7, 41], PEG is relatively easy available in a range of well-defined molar masses with low dispersity. Therefore, chemically cross-linked hydrophilic coatings composed of a PEG-diol and a tri-isocyanate cross-linker were selected as model system. The effect of the PEG-diol precursor mass on water uptake, indentation modulus, surface hydrophilicity and macroscopic aqueous friction behavior of the water-swollen hydrophilic PU coatings against a glass counter surface was studied. For the latter, a custom-made tribology setup was used. Based on the calculated mesh size (taking into

account corrections for network defects and a properly constrained coating network deformation during swelling) and measured friction behavior, an empirical model for the description of the obtained friction data is deduced.

# Materials and methods

## Materials

Poly(ethylene glycol) (PEG) with varying molar mass ($M_n$ = 1000, 2000, 4000, 6000 and 10000 g mol$^{-1}$) (Sigma-Aldrich) (all PDI < 1.04 (SEC)) was dried before use, at room temperature in a desiccator with $P_2O_5$ as desiccant for at least 72 h. Further purification of PEG via azeotropic distillation did not significantly improve the purity of the compounds, as shown by NMR. Trimerized hexamethylene diisocyanate (tHDI) (equivalent functional weight of 183 g mol$^{-1}$ NCO (manufacturer value)) was kindly provided by Perstorp as tolonate HDT-LV2 and used as received. Cyclohexanone (99.8%) (Sigma-Aldrich) was dried over molecular sieves before use. Dibutyltin dilaurate (95%) (DBTDL) and (3-aminopropyl)triethoxysilane (> 98%) (APTES) were purchased from Sigma-Aldrich and used as received.

## Coating preparation

The coating preparation procedure was optimized to yield PEG-based PU coatings with sufficient adhesion to a glass substrate when immersed in water. Contact of oxygen with the network precursors was minimized as much as possible to prevent possible degradation of the polymers during network preparation. Therefore, every time a vial was opened during the whole preparation procedure, it was thoroughly flushed with argon after opening and before closure. Moreover, the lid was wrapped with parafilm tape after closure. All glassware was dried in an oven at 100 °C for at least 14 h prior to use. The coatings were applied on soda-lime glass substrates (extra low iron content, 49 × 49 × 1 mm$^3$) provided with a primer layer.

Primer precursor stock solutions (typically 10 ml) of PEG 6000 g mol$^{-1}$ (10 wt%) and of tHDI (50 wt%) were made by dissolving PEG and tHDI in cyclohexanone at 55 °C and room temperature, respectively. This was done in closed glass vials under an argon blanket and continuous stirring. The primer formulation solutions (typically 10 ml) were prepared in a glass vial by mixing the primer precursor stock solutions at 55 °C under an argon blanket after which APTES was added in a NCO/OH/NH$_2$ molar ratio of 1.3:1:0.3 and stirred for 1 h before application. The glass substrates were cleaned by rubbing with a tissue embedded with ethanol and dried in an oven at 100 °C for at least 14 h. Prior to use, they were given a UV-ozone treatment (Novascan PSD-UVT) for 10 min and preheated at 65 °C after which the primer solution (0.4 ml) was spin-coated (Laurell WS-650SX-6NPP/LITE) for 15 s at 1000 rpm. The coated substrates were positioned on top of a preheated (65 °C) heating element placed in a chamber (with a volume of approximately 1.5 dm$^3$), which after closure was continuously flushed with dry N$_2$ (± 150 l h$^{-1}$ at 1 bar). The primers were formed by a solvent evaporation step of 90 min at 65 °C to remove both the solvent as well as the oxygen present, followed by a final cure step of 14 h at 150 °C under a dry N$_2$ flow (± 150 l h$^{-1}$ at 1 bar). The cured primers were immersed in demineralized water for at least 14 h to extract the extractable components. The extracted primers were dried at ambient conditions and further dried at 20 mbar at 40 °C for at least 2 h before applying the coatings.

For the coatings, coating precursor stock solutions (typically 10 ml) of PEG (10–15 wt%) and of tHDI (50 wt%) in cyclohexanone were made by dissolving PEG and tHDI in cyclohexanone at 55 °C and room temperature, respectively. This was done in closed glass vials under an argon blanket and continuous stirring. The coating formulation solutions (typically 3 ml) were prepared in a glass vial by mixing the coating precursor stock solutions at 55 °C under an argon blanket. The NCO/OH molar ratio of each formulation was kept at 1.1 to ensure full conversion of the OH-groups. Just before application, the coating solutions were heated to 65 °C and were mixed with a 10 mg ml$^{-1}$ DBTDL solution in cyclohexanone (approximately 0.2 wt% DBTDL, with respect to the weight of the coating precursors). Prior to the coating application, the extracted and dried primed substrates received a UV-ozone treatment (Novascan PSD-UVT) for 12 s and were put on a preheated (65 °C) coating stage. The coating solutions (0.25 ml) were barcoated by hand using a spiral wire bar resulting in a wet-film thickness of approximately 40 μm. The wet coatings were positioned on top of a

preheated (65 °C) heating element placed in a chamber (with a volume of approximately 1.5 dm$^3$), which after closure was continuously flushed with dry N$_2$ ($\pm$ 150 l h$^{-1}$ at 1 bar). Subsequently, the coatings were formed by a solvent evaporation step of 90 min at 65 °C to remove both the solvent as well as the oxygen present, followed by a final cure step of 4 h at 125 °C under a dry N$_2$ flow ($\pm$ 150 l h$^{-1}$ at 1 bar). The cured coatings were immersed in demineralized water for at least 14 h to extract the extractable components. Thereafter, the extracted coatings were dried at ambient conditions and further dried at 20 mbar at 40 °C for at least 2 h and stored in a moisture-free desiccator. From here onward, purely PEG-diol-based PU coatings will be named PUPEG($M_n$ of used PEG).

## Coating characterization

### Attenuated total reflection Fourier transform infrared spectroscopy (ATR-FTIR)

Fourier transform infrared spectroscopy (FTIR) absorbance spectra of cured networks were recorded in attenuated total reflection (ATR) mode using a Varian Excalibur FTIR-3100 equipped with a diamond Specac Golden Gate ATR stage. Given the large overlap of the C=O urethane stretch vibration (1720 cm$^{-1}$) and the isocyanurate C=O stretch vibration (1675 cm$^{-1}$) present in the networks, and moreover the C–N urethane stretch vibration band (1550 cm$^{-1}$) being located in the fingerprint region, a reliable quantitative analysis of NCO to urethane conversion from the IR absorbance spectra is impracticable. Therefore, only the disappearance of the N=C=O asymmetric stretch vibration at 2270 cm$^{-1}$ was used to analyze the NCO conversion of the cured networks at the surface.

### Coating thickness

A Bruker Veeco Dektak 150 profilometer was used to measure the dry thickness of a coating. A scratch was made to completely remove a small part of the coating, after which the height profile across the interface of the exposed substrate and the coating was measured at four random locations.

### Static captive air bubble contact angle measurements in water

The hydrophilicity of the coatings was evaluated by static captive air bubble contact angle CA$_{air}$ measurements in water using a Data Physics OCA 30 goniometer. A coating, swollen to equilibrium for at least 14 h, was placed upside-down in a glass container filled with demineralized water. An air bubble with a volume of approximately 4 μl was placed on the coating surface after which the static air contact angle was measured. The static CA$_{air}$ was measured at five different locations per sample, and the contact angles presented are the average value for the sample and their mean absolute deviation for each coating type. The mean absolute deviation for each coating was of the same order as the mean absolute deviation between means of samples of coatings (of the same type).

### Experimental network swelling characterization

The weights of the substrate, the primer and the coating were measured before and after each application, curing and extraction step. The amount of extractable material $L$ is calculated via $L = ((m_i - m_0)/m_i) \cdot 100\%$, where $m_i$ and $m_0$ are the initial weights of a coating after curing and of an extracted dry coating, respectively. Any extracted coating was immersed in demineralized water again to swell to equilibrium for at least 14 h. The swollen weight of the coating $m_{eq}$ was measured directly after the coating was taken out of the water and after gentle removal of all excess water with absorbing lint free paper. Based on the water uptake, the polymer network volume fraction $\varphi_n$ in a swollen coating was calculated using

$$\varphi_n = V_n/V = V^0/V = 1/Q \tag{1}$$

where $V$ is the total volume of the swollen coating, $V_n$ the dry volume of the coating, and $V^0$ the initial volume of the coating before swelling. Here, we equated $V_n$ and $V^0$ since the coating is cross-linked in the absence of a solvent. The volumetric equilibrium swelling ratio $Q$ is calculated from the measured water uptake via

$$Q = \frac{V}{V^0} = 1 + \frac{\rho_n}{\rho_{H_2O}}\left(\frac{m_{eq}}{m_0} - 1\right) \tag{2}$$

where $\rho_{H_2O}$ is the density of water (1 g cm$^{-3}$) and $\rho_n$

the density of the dry coating. Values for $\rho_n$ slightly differ for different network formulations, given the different overall network composition. Therefore, the value for $\rho_n$ of each different dry network is estimated via $\rho_n = \rho_{PEG} \cdot \varphi_{EG}^{vol} + \rho_{tHDI}\left(1 - \varphi_{EG}^{vol}\right)$, assuming no excess volume upon mixing and polymerization, where $\rho_{PEG}$ (= 1.2025) and $\rho_{tHDI}$ (= 1.3349) are the densities of the PEG network precursors and tHDI in the network, respectively. Both were calculated with Molecular Modeling Pro software [42] using the molecular volumes [43]. The quantity $\varphi_{EG}^{vol}$ is the volume fraction of ethylene glycol (EG) units in the dry network and is calculated from the mass ratio of the network precursors via their densities by

$$\frac{1}{\varphi_{EG}^{vol}} = 1 + \frac{\rho_{PEG}}{\rho_{tHDI}} \cdot \left(\frac{1}{\varphi_{EG}} - 1\right) \tag{3}$$

where $\varphi_{EG} = m_{PEG}/(m_{PEG} + m_{tHDI})$ is the initial weight fraction of EG units in the dry network with $m_{PEG}$ and $m_{tHDI}$ the masses of the precursors in the coating formulation.

### Mechanical characterization: immersed nano-indentation

Nano-indentation measurements on completely immersed and swollen coatings were taken using an optical interferometer-based Piuma Nanoindenter (Optics11 B.V. Amsterdam (NL)). Two different probes (Optics11 B.V.) were used throughout the measurements of the whole dataset. The probes were equipped with a spherical glass tip (with a radius of 19.0 and 19.5 μm, respectively) connected to a cantilever (with a stiffness of 17.3 and 18.9 N m$^{-1}$, respectively). An Optics11 OP1550 interferometer (laser wavelength of 1550 nm) was used to detect the sample deformations by detecting the cantilever deflections completely immersed in water. Each coating, swollen to equilibrium for at least 14 h, was immersed in a petri dish filled with demineralized water after which the indentation modulus was measured at 5 random locations. Generally, each indentation was done by a piezoelectrical controlled downward movement of the indenter head of 18.6 μm at a velocity of 1.86 μm s$^{-1}$. The probe was held at the maximum depth for 5 s after which it was withdrawn within 1 to 2 s. The load–displacement curve of each indentation was recorded, and the effective indentation modulus $E^*$ was calculated

using standard Hertzian contact mechanics for a rigid indenter and an elastic half space [44, 45] as given by

$$a^3 = \frac{3}{4}\frac{PR}{E^*} \quad \text{and} \quad \delta = \frac{a^2}{R} \tag{4}$$

where $a$ is the radius of the circle of contact, $P$ the applied load, $R$ the radius of the indenter, and $\delta$ the indentation depth. For the calculation of the indentation modulus of the top surface of the coating $E$, the value of $E^*$ was taken at 5% of the total load to ensure an indentation depth to film thickness ratio $\delta/h < 0.05$, in order to minimize the effect of the modulus of the substrate on the measured coating response [46]. Since the indenter is position controlled with a fixed cantilever stiffness, the absolute depth of the indentation into the coating surface varied for all coatings. Nevertheless, even for the coatings with the lowest $E$, the absolute indentation depth at 5% of the maximum load did not exceed a depth of 1300 nm. The indentation modulus $E$ is calculated from the measured $E^*$ via

$$1/E^* = \left[(1 - \nu^2)/E\right] + \left[(1 - \nu_{ind}^2)/E^{ind}\right] \tag{5}$$

where $E^{ind} \approx 70$ GPa is the modulus of the glass indenter, $\nu_{ind} \approx 0.25$ is Poisson's ratio of the indenter and $\nu$ is Poisson's ratio of the coating, taken as 0.5 as for an ideal rubber. The second term on the right hand side of Eq. (5) can actually be neglected since $(1 - \nu^2)/E >> (1 - \nu_{ind}^2)/E^{ind}$ because $E$ is in the order of 1–10 MPa.

### Mechanical characterization: immersed tribology

An AR-1000 N Rheometer (TA Instruments) was adapted to be able to use it as a tribology setup for the measurement of the macroscopic friction response of the coatings immersed in water. An overview of the used equipment is shown in Fig. 2. The indenter head contains three spherical optical grade N-BK7 glass lenses (Borosilicate Crown glass), with a large radius of curvature ($R = 0.25$ m) and a diameter of 0.025 m, mounted with the centers of the lenses located in a triangular arrangement, at 0.0145 m out of the center of the indenter head. This shallow curvature is chosen to ensure a large contact area between the indenters and the coating (in the order of mm$^2$ per lens), thereby minimizing the contact pressure (in the order of 50–150 kPa) and ensuring a close-to-homogeneous stress distribution in the deformed coatings. The indenter head is mounted to the rotating shaft of
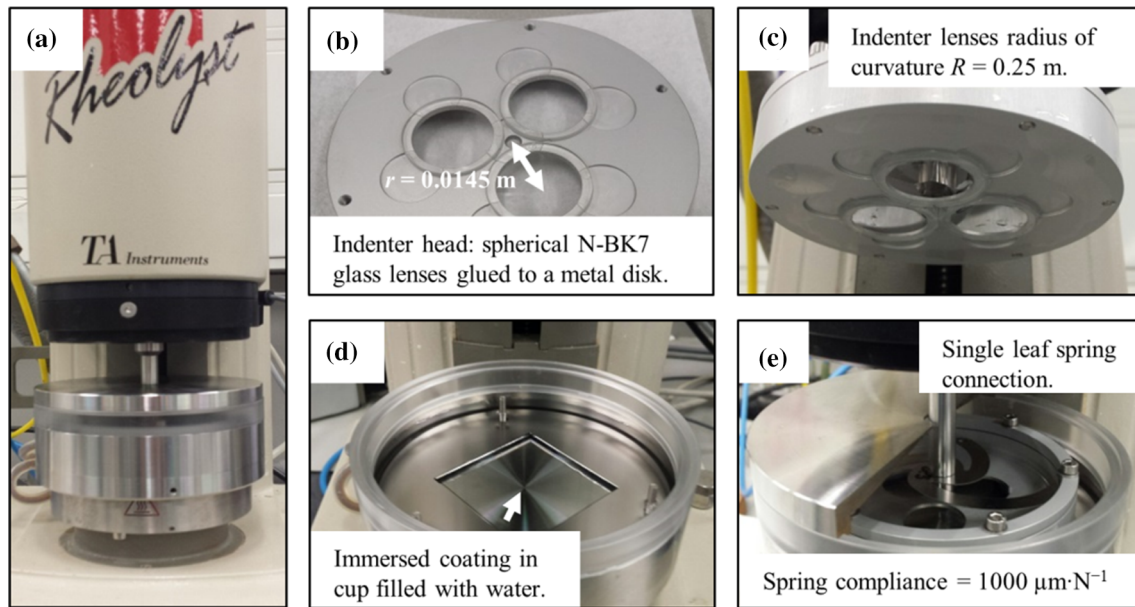
**Figure 2** Overview of the custom-made tribology setup used in this work. **a** Front view of the adapted rheometer. **b** and **c** Bottom view of the indenter head showing the three spherical lenses used as indenters. Radius of curvature of the lenses is 0.25 m. The center of the lenses is placed 0.0145 m out of the center of the indenter head. **d** Top view of the cup mounted on the bottom plate of the rheometer containing the water and immersed sample. **e** Top view of the indenter head which shows the single leaf spring connection (spring compliance is 1000 μm N$^{-1}$) between the indenter head and the rotating shaft of the rheometer.

the rheometer via a single, specially designed leaf spring (with a spring compliance of 1000 μm N$^{-1}$) for making each of the lenses carefully follow the surface of the coating with equal contact forces, while assuring that the triangle center is kept at the shaft axis. A cup which can contain the measurement medium (typically, demineralized water), and the immersed coating was mounted on the bottom plate of the rheometer.

The tribometer can be operated in a velocity window between $10^{-3}$ to 70 rad s$^{-1}$ and up to a normal load of 20 N, with a bandwidth of 0.1 N around the set-point at a constant longitudinal position of the rotating shaft. Forces are recorded with a normal force resolution of 0.0057 N and a torque resolution of 0.01 μN m. All series of measurements were taken in demineralized water at approximately 20 °C.

Coatings, swollen to equilibrium for at least 14 h, were immersed and equilibrated in the setup at a normal load of 0.5 N for 30 min prior to the measurements. Each measurement was divided stepwise into different constant velocity segments (ranging from $10^{-3}$ to 30 rad s$^{-1}$). Depending on the rotation speed in a velocity segment test, a full circular path at the sample surface was probed either once (at very low speeds) or more often (at high speeds) (See

Supporting Information (SI) SI-1 for an overview of the length of each selected velocity segment). A stationary equilibration time of 1 min, at the set normal load, was allowed between each velocity step. If a sample was measured at different normal loads, the velocity segments at the lowest load were programmed first, after which the same run at a higher load was programmed with 30 min of stationary equilibration, at the subsequent normal load, in between. The absolute applied normal load and measured torque were averaged over the total segment time, with the first 30 s excluded. From the resulting average torque $T_\omega$ and normal load $F_N$, the coefficient of friction (CoF) was calculated via

$$\text{CoF} = (T_\omega/r)/F_N \tag{6}$$

where $r = 0.0145$ m is the distance between the center of the indenter head and the center of a lens. For an example of raw data of a typical measured friction response, see SI-2.

# Theory

## Mesh size calculation

In order to relate the network architecture to the friction behavior of the swollen coatings, an accurate calculation of the molar mass between cross-links $M_c$ is needed for an estimation of the absolute mesh size $\xi$ of the coatings. The mesh size $\xi$ of a network is a structure parameter which gives the average distance between two neighboring cross-links (see Fig. 3).

Once the average molar mass between cross-linking points in the structure is known, the mesh size of the structure can be calculated using the intrinsic characteristics of the polymer between the cross-links [47]. The parameter $\xi$ in the swollen network is calculated from the root-mean-square end-to-end distance between the cross-links $(\bar{r}_0^2)^{1/2}$ via

$$\xi = \varphi_n^{-1/3}(\bar{r}_0^2)^{1/2} \tag{7}$$

where $(\bar{r}_0^2)^{1/2}$ is given by

$$(\bar{r}_0^2)^{1/2} = l(N_b M_c/M_m)^{1/2} C_\infty^{1/2} \tag{8}$$

with $l$ the average bond length of the PEG backbone taken as 1.464 Å [48, 49], $C_\infty$ the characteristic ratio of PEG (typically 4.0) [48, 50], $N_b$ the number of bonds per ethylene glycol unit in the backbone (3), and $M_m$ the molar mass of the ethylene glycol unit (44 g mol$^{-1}$).
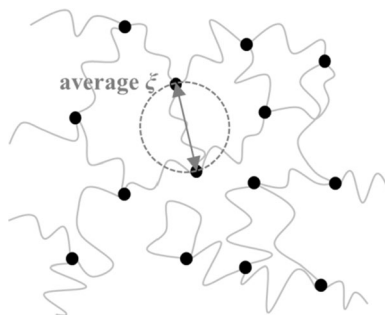


**Figure 3** Schematic depiction of a cross-linked network with mesh size $\xi$. The average mesh size of a network is based on the root-mean-square end-to-end distance between two neighboring cross-links and the polymer volume fraction of the swollen network.

## Calculation of $M_c$ assuming in-plane constrained swelling

The $M_c$ of a swollen polymer network can be calculated via water uptake (swelling) experiments as well as from mechanical data [51]. Various network models have been developed to relate topological molecular interpretations of the network structure to the (swelling) deformation behavior of elastomeric networks [51–53]. Of all models available, the mechanical behavior of highly swollen polymer networks is shown to be best described by the phantom model [51, 54–58]. Classically, the phantom network model does not take into account the presence of imperfections in the network structure. Our previous work [59] has shown an effective method to obtain correction factors to the ideal network parameter relations [51] which are used in the phantom model to obtain an accurate value for $M_c$ of PEG-based PU networks. The proposed correction factors are calculated using the Miller–Macosko–Vallés (MMV) approach [60–62]. The aspect ratio $h/l$ of the coatings is in the order of $10^{-4}$, and since the coatings are adhering to the substrate, they are limited to swell out-of-plane only and are constrained in-plane (i.e., the x-y plane). By making use of the proper swelling deformation and the use of corrections for network imperfections, the expression for the average $M_c$ based on swelling experiments for an in-plane constrained swelling deformation $M_c^{\text{swell, con}}$ is given as (see SI-3 for a derivation)

$$M_c^{\text{swell, con}} = -\frac{\rho_n\left(\alpha - \left(\frac{2}{f}\right)\beta\right)V_s\left(\frac{\varphi_n}{\varphi_{n_0}}\right)^{-1}}{\ln(1 - \varphi_n) + \varphi_n + \chi\varphi_n^2} \tag{9}$$

where $\rho_n$ is the dry network density, $V_s$ the molar volume of the solvent (18.0685 cm$^3$ for water), $\varphi_n$ the polymer volume fraction in the swollen network, $\varphi_{n_0}$ the polymer volume fraction during the network formation (which is unity in this work since the networks are formed after evaporation of the solvent), $f$ the functionality of the network junctions, $\chi$ the Flory–Huggins water–polymer interaction parameter, $\alpha$ the fraction of elastically active network chains in the network and $\beta$ the fraction of elastically active cross-link molecules. Both correction factors are calculated using the Miller–Macosko–Vallés (MMV) approach for an $A_5A_3B_2$ system (see SI-4), in which allophanate formation has been taken into account (see SI-5). The parameter $\chi$ is taken as a linear

function of $\varphi_n$ ($\chi = 0.46034 + 0.4195\varphi_n$) based on data of Gnanou et al. [63] (see SI-6).

In a similar fashion, the average $M_c$ based on indentation experiments for an in-plane constrained swelling deformation $M_c^{\text{indent, con}}$ can be derived and is given by

$$M_c^{\text{indent, con}} = 3RT\rho_n\left(\alpha - \left(\frac{2}{f}\right)\beta\right)\left(\frac{\varphi_n}{\varphi_{n_0}}\right)^{-1}/E \qquad (10)$$

where $R$, $T$ and $E$ are the gas constant, the temperature and the indentation modulus, respectively. See SI-7 for a derivation of Eq. (10).

# Results and discussion

## Coating preparation and network properties

PEG-based PU coatings with an average dry film thickness of 6–7 μm were studied in this work as model systems (see SI-8 for pictures of coatings). It is of crucial importance for a reliable comparison of the lubricity of coatings to ensure a reliable and comparable network formation for the coatings. IR absorption spectra of several coatings taken showed a complete absence of the NCO band at 2270 cm$^{-1}$ after cross-linking (see SI-9 for several typical spectra). This absence of NCO proves complete NCO conversion. Nevertheless, the prepared coatings contained a small fraction of extractable material as given in Table 1. Although not completely negligible, the weight fractions of extractable material are small enough to conclude that qualitatively good and similar coating network structures were formed. This is confirmed by the significant differences and clear trends observed for the measured network properties conform expectation, such as water uptake,

indentation modulus $E$ and surface hydrophilicity. The latter is assessed via the static air contact angle in water $\text{CA}_{\text{air}}$. See Table 1 and Fig. 4 for the data and SI-10 for typical indentation curves as obtained by immersed nano-indentation of the swollen coating surface. The amount of extractable material was taken into account in the calculations of the molar mass $M_c$ between cross-links in the next section.

The measured trends of increasing volumetric swelling ratio $Q$ and decreasing indentation modulus $E$ for the coatings with increasing $M_n$ of the PEG network precursor, as shown in Fig. 4a, are consistent with each other and conform expectation upon decreasing the cross-link density of the coating networks. Furthermore, although the differences in $\text{CA}_{\text{air}}$ are small (Fig. 4b), an increase is observed for coatings prepared with larger $M_n$ value precursors (thus larger $\varphi_{\text{EG}}$), indicating a somewhat larger hydrophilicity. Note that a higher air bubble contact angle in water means a lower water contact angle, $\text{CA}_{\text{water}} = 180° - \text{CA}_{\text{air}}$.

Both the swelling and the indentation data were used to calculate the molar mass between cross-links $M_c$ of the coatings, taking into account in-plane constrained swelling deformation (see "Calculation of $M_c$ assuming in-plane constrained swelling" section). Both sets of values for $M_c$ are given in Table 2 and Fig. 5 and show that the data from swelling and indentation data are similar. Moreover, the slope of the $M_n$ versus $M_c$ is close to unity, as expected for networks prepared via an end-linking reaction of the polymer precursors with multifunctional cross-linkers. This confirms that the relation between the network parameters and the swelling deformation is well described theoretically by an elastic in-plane constrained deformation. Assuming isotropic

**Table 1** Amount of extractable material $L$, mass ratio $m_{\text{eq}}/m_0$, ethylene glycol fraction in dry network $\varphi_{\text{EG}}$, dry network density $\rho_n$, volumetric swelling ratio $Q$, indentation modulus $E$ and static captive air bubble contact angle in water $\text{CA}_{\text{air}}$ of the prepared PUPEG-based

coatings. Number of samples per coating type varies between 4 and 6. The dry thickness of the coatings is 6–7 μm. The error shows the mean absolute deviation from the mean value

| PUPEG | $L$ (%) | $m_{\text{eq}}/m_0$ (g/g) | $\varphi_{\text{EG}}$ (-) | $\rho_n$ (g cm$^{-3}$) | $Q$ (V/V$^0$) | $E$ (MPa) | $\text{CA}_{\text{air}}$ (°) |
|---|---|---|---|---|---|---|---|
| PEG1000 | $2.5 \pm 1.3$ | $1.80 \pm 0.07$ | 0.713 | 1.238 | $1.96 \pm 0.12$ | $6.2 \pm 0.8$ | $142 \pm 1$ |
| PEG2000 | $0.8 \pm 0.4$ | $2.28 \pm 0.15$ | 0.833 | 1.223 | $2.57 \pm 0.18$ | $3.8 \pm 0.1$ | $146 \pm 1$ |
| PEG4000 | $1.4 \pm 0.4$ | $2.78 \pm 0.24$ | 0.908 | 1.214 | $3.16 \pm 0.29$ | $2.3 \pm 0.2$ | $147 \pm 1$ |
| PEG6000 | $2.6 \pm 1.2$ | $3.12 \pm 0.12$ | 0.937 | 1.210 | $3.45 \pm 0.31$ | $1.9 \pm 0.2$ | $148 \pm 1$ |
| PEG10000 | $5.1 \pm 1.3$ | $3.53 \pm 0.35$ | 0.961 | 1.207 | $4.05 \pm 0.42$ | $1.1 \pm 0.1$ | $150 \pm 1$ |

**(a)**



**(b)**
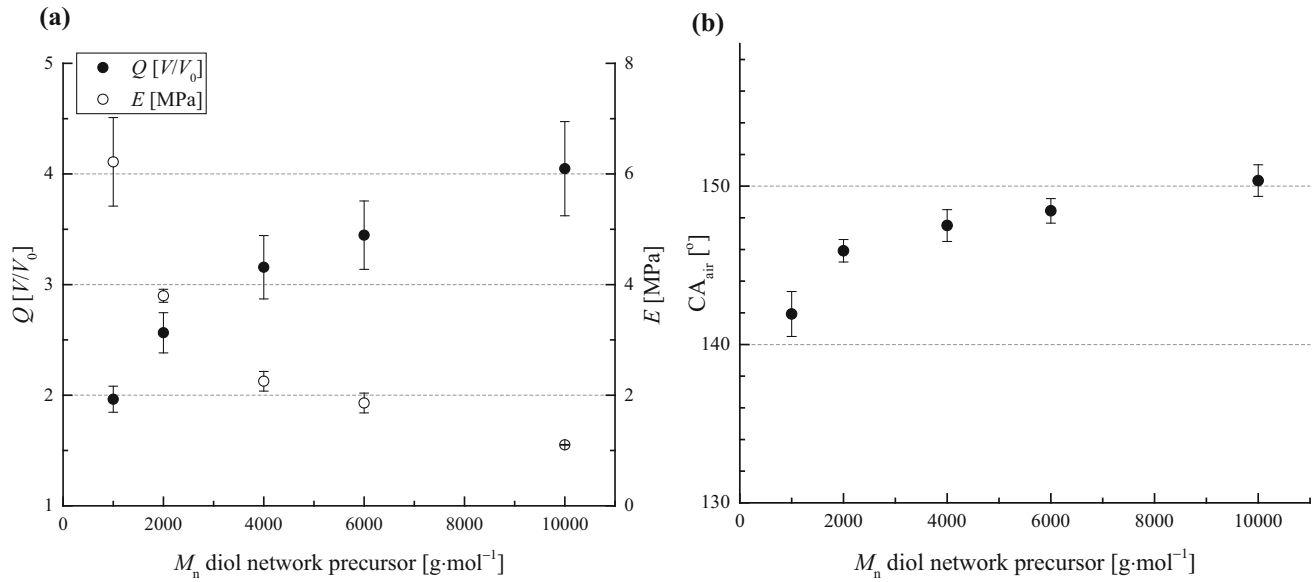


**Figure 4** Experimental values for properties of the PEG-based PU coatings swollen to equilibrium in water. **a** Mean volumetric swelling ratio Q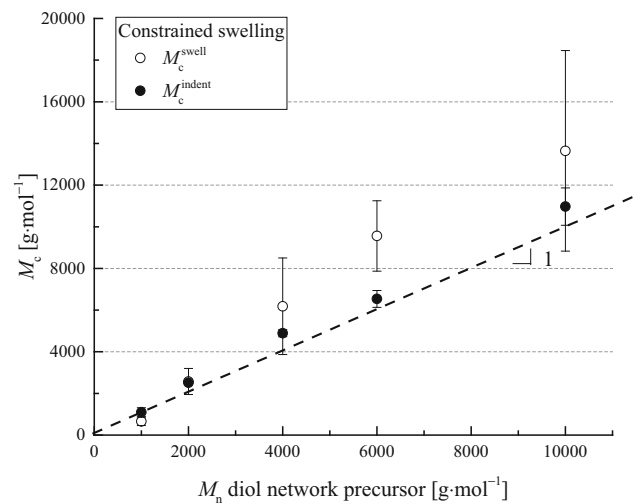 and indentation modulus E. **b** Mean air contact angle measured using a captive air bubble in water. The error bars show the mean absolute deviation.

**Table 2** Calculated mean $M_c^{swell}$ and $M_c^{indent}$ for the swollen PEG-based PU coatings assuming in-plane constrained swelling using Eqs. (9) and (10) with $f = 3.75$. The error shows the mean absolute deviation

| PUPEG | $M_c^{swell, con}$(g mol$^{-1}$) | $M_c^{indent, con}$(g mol$^{-1}$) |
|---|---|---|
| PEG1000 | $659 \pm 201$ | $1098 \pm 216$ |
| PEG2000 | $2573 \pm 623$ | $2514 \pm 62$ |
| PEG4000 | $6183 \pm 2319$ | $4889 \pm 170$ |
| PEG6000 | $9559 \pm 1690$ | $6537 \pm 405$ |
| PEG10000 | $13644 \pm 4813$ | $10969 \pm 896$ |



**Figure 5** Calculated mean $M_c^{swell}$ and $M_c^{indent}$ for the swollen PEG-based PU coatings for in-plane constrained swelling (e.g., in the x-y plane) using Eqs. (9) and (10) with $f = 3.75$. The error bars show the mean absolute deviation.

swelling of the coatings would severely underestimate the $M_c$-values by a factor of 2–4 (see SI-11).

The errors on the mean values for $M_c$ are significantly larger for $M_c^{swell, con}$ compared to those for $M_c^{indent, con}$, especially for the coatings which contain higher $M_n$ precursors. This is most likely due to the high sensitivity of $M_c^{swell, con}$ on the polymer–water interaction parameter $\chi$. Since $\chi$ is a function of the polymer volume fraction $\varphi_n$, $M_c^{indent, con}$ is less sensitive toward deviations in the measured water uptake compared to $M_c^{swell, con}$. Therefore, the values for $M_c^{indent, con}$ were used to calculate the mesh size $\xi$ of the PEG-based PU coatings (Table 3).

## Friction behavior of water-swollen PEG-based PU coatings

The lubricity of the coatings was measured with our custom-made immersed tribology setup (see "Mechanical characterization: immersed tribology" section). The calculated average CoFs for a normal load of 0.5 N for each velocity are given in Fig. 6. The global trend shows a lower CoF at higher loads, as

**Table 3** Mean mass between cross-links $M_c^{\text{indent, con}}$ and corresponding mean mesh size $\xi$ of the PEG-based PU coatings. The error shows the mean absolute deviation from the mean value

| PUPEG | $M_c^{\text{indent, con}}$ (g mol$^{-1}$) | $\xi$ (nm) |
|---|---|---|
| PEG1000 | $1098 \pm 216$ | $3.2 \pm 0.3$ |
| PEG2000 | $2514 \pm 62$ | $5.3 \pm 0.1$ |
| PEG4000 | $4889 \pm 170$ | $8.0 \pm 0.4$ |
| PEG6000 | $6537 \pm 405$ | $10.1 \pm 0.3$ |
| PEG10000 | $10969 \pm 896$ | $13.7 \pm 0.9$ |
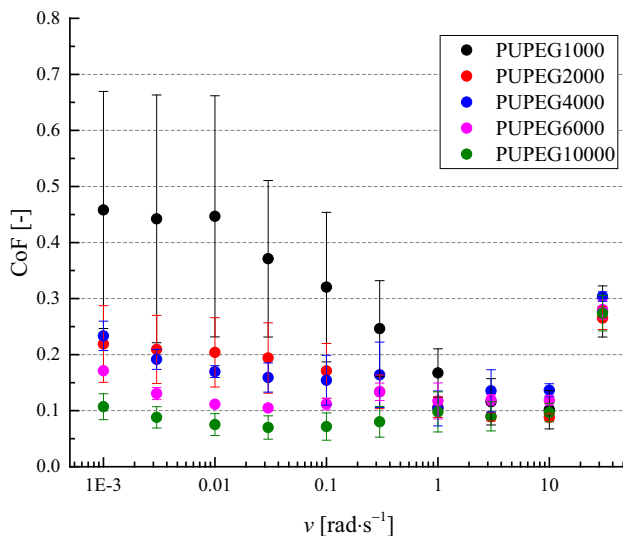


**Figure 6** Mean coefficient of friction (CoF) versus angular velocity $v$ of water-swollen PEG-based PU coatings with varying precursor $M_n$, immersed in demineralized water against a glass counter surface measured at a normal load of 0.5 N. 1 rad s$^{-1}$ = 0.0145 m s$^{-1}$. The error bars show the mean absolute deviation.

expected for swollen hydrophilic networks [21]. Most coatings could be measured at a normal load of 0.5 N without being damaged, whereas experiments at higher loads often ruptured the coatings during the measurement, resulting in visible damage and (partial) removal of material in the sliding path. Since shear stresses in the coating are higher at higher loads, this is most likely the cause of the rupture. Given the limited amount of data at higher loads, we focus our study on the lubricating properties of the coatings at a normal load of 0.5 N.

Two different friction regimes can be clearly identified in Fig. 6. At velocities above the transition at 3 rad s$^{-1}$, the hydrodynamic regime, the friction response of all networks is independent of the

network architecture as the indenters lose contact with the coating surface and the friction response is governed by the viscosity of the medium in the gap [21, 64]. Below the transition, the interaction regime, the indenters make actual contact with the coating and differences in network architecture give rise to a difference in friction response of the coating. A clear trend of a decreasing CoF upon increasing the PEG-diol precursor $M_n$ can be observed. This behavior agrees well with the work of Sawyer and coworkers on hydrogel-hydrogel friction which shows a decreasing CoF upon increasing mesh size of their prepared polyacrylamide gels [34, 35]. Moreover, the network mesh size is known to influence the friction behavior of gels, as described by the attraction–adsorption model of Gong and Osada [24]. As stated in Introduction, in the interaction regime using the proposed mechanism, friction originates from a contribution of the elastic deformation of the adsorbed polymer chains to the surface and a contribution of the lubrication of the hydrated layer of the polymer network. The former is similar to the adhesive friction of rubbers described by Schallamach [25], in which the peak stress increases with increasing modulus of elastomers [65]. If one compares the overall friction behavior of the studied coatings with these theories of rubber friction and gel friction, qualitatively similar behavior is observed.

## Mesh size–friction behavior relation of PEG-based PU coatings

The PEG-based PU coatings vary in absolute PEG content. Under the assumption that the aqueous friction behavior of the coatings is governed by the hydrophilic part of the flexible chains between the more rigid cross-linker molecules, the actual calculated mesh size $\xi$ should be scaled by the overall PEG fraction of the polymer network $\varphi_{\text{EG}}$ (see SI-12 for a depiction). The empirical or descriptive model, as elucidated in this section, indeed turns out to give the best fit with the measured CoF when developed based on $\xi\,\varphi_{\text{EG}}$ instead of $\xi$. Therefore, only the model development based on $\xi\,\varphi_{\text{EG}}$ is presented.

Once the mesh size is known, it can be related to the measured friction response. The measured CoF is plotted against the calculated mesh size $\xi\,\varphi_{\text{EG}}$ in Fig. 7 for various sliding velocities. An approximately linear relation between the log(CoF) and log($\xi\,\varphi_{\text{EG}}$) values is observed, suggesting power law
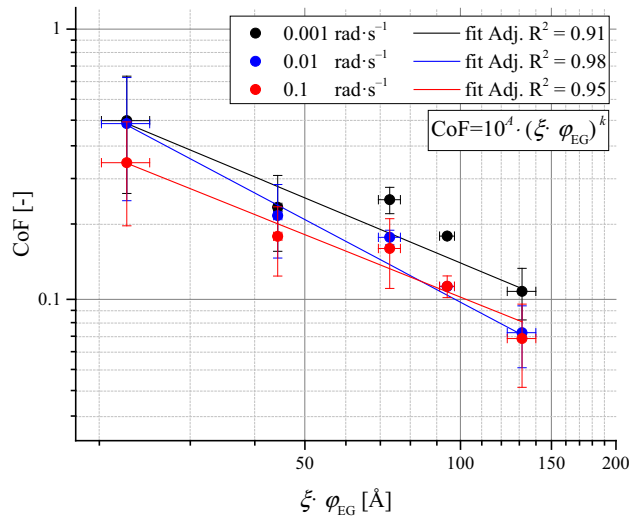
**Figure 7** Mean coefficient of friction (CoF) at different sliding velocities versus calculated mesh size $\xi \bullet \varphi_{EG}$ of the water-swollen PEG-based PU coatings. CoF measured at a normal load of 0.5 N.

scaling between $\xi \varphi_{EG}$ and the CoF. The fitting parameters $(A,k)$ and the value of the adjusted $R^2$ (Adj. $R^2$) of these linear fits are given in Table 4. The Adj. $R^2$ values indicate that the fit describes the relation reasonably well, especially for velocities below 0.3 rad s$^{-1}$, which is, as noted, the transition point to the hydrodynamic regime. The data were also plotted in a semi-log plot to assess whether the friction behavior would be better described by an exponential relation, but the associated Adj. $R^2$ values (see SI-13) are significantly lower. Therefore, we conclude that power law scaling CoF $= 10^A(\xi \ \varphi_{EG})^k$ describes the relation best.

When analyzing these results, it turned out that there is a strong correlation between the values of the

**Table 4** The values for $A$ and $k$ of the fits of log[CoF] versus log[$\xi \cdot \varphi_{EG}$] at various sliding velocities $v$ for the PEG-based PU coatings and the adjusted $R^2$ value for the weighted linear fit. 1 rad s$^{-1}$ = 0.0145 m s$^{-1}$

| Velocity [rad•s$^{-1}$] | $A$ | $k$ | Adj. $R^2$ |
|---|---|---|---|
| 0.001 | $0.73 \pm 0.19$ | $-0.80 \pm 0.12$ | 0.91 |
| 0.003 | $0.87 \pm 0.18$ | $-0.91 \pm 0.12$ | 0.94 |
| 0.01 | $1.02 \pm 0.10$ | $-1.02 \pm 0.07$ | 0.98 |
| 0.03 | $0.77 \pm 0.12$ | $-0.89 \pm 0.07$ | 0.97 |
| 0.1 | $0.54 \pm 0.14$ | $-0.77 \pm 0.09$ | 0.95 |
| 0.3 | $0.07 \pm 0.25$ | $-0.51 \pm 0.14$ | 0.74 |
| 1 | $-0.42 \pm 0.15$ | $-0.27 \pm 0.09$ | 0.69 |
| 3 | $-0.84 \pm 0.23$ | $-0.06 \pm 0.13$ | $-0.25$ |

parameter $k$ in CoF $= 10^A(\xi \ \varphi_{EG})^k$ (i.e., the slope of the fits in Fig. 7) and the sliding velocity $v$ (Fig. 8a). This relation between $k$ and log[$v$] can be described with a parabolic function ($B_0 = 1.16 \pm 0.16$, $B_1 = 1.04 \pm 0.12$, $B_2 = 0.130 \pm 0.018$, Adj. $R^2 = 0.969$). The fitting parameter $10^A$ (the (fictitious) intercepts of the fits in Fig. 7) was also found to strongly correlate with $k$ (Fig. 8b): a clear linear relation between $A$ and $k$ is observed ($C_0 = -0.883 \pm 0.052$, $C_1 = -1.906 \pm 0.064$, Adj. $R^2 = 0.992$).

Given these strong correlations, an empirical descriptive model for these PEG-based PU coatings is given, using $B_0 = 1.16$, $B_1 = 1.04$, $B_2 = 0.13$, $C_0 = -0.883$ and $C_1 = -1.906$, by

$$\text{CoF} = 10^A(\xi \cdot \varphi_{EG})^k \text{ with } 10^A = 10^{C_0+C_1 \cdot k} \text{ and } k$$
$$= B_0 + B_1 \log[v] + B_2 \log[v]^2 \qquad (11)$$

This equation for the description of the friction behavior only depends on the corrected mesh size and the sliding velocity for this type of PEG-based PU coating. To assess this empirical model, Fig. 9 shows the fit curves up to 4 rad s$^{-1}$ together with the measured data. We conclude that the model succeeds in describing the decreasing of CoF with increasing polymer mesh size rather quantitatively up to the transition to the hydrodynamic lubrication regime. The largest deviation seems to exist at the lowest velocity measured, 14.5 µm s$^{-1}$. This velocity is close to the operating limit of the tribometer used. Furthermore, the whole sliding path of each coating is measured only once during a tribology measurement at this velocity. Therefore, the deviation at this velocity is believed to be due to experimental limitation and increased experimental error.

As stated before, the fitting procedures were also done for the uncorrected mesh size $\xi$. The resulting total residual sum of squares (RSS) for the empirical model CoF($\xi$) turns out to be larger than the total RSS for the model CoF($\xi \ \varphi_{EG}$) (see SI-14). A further extension of the $k$ versus log[$v$] relationship to a third-order polynomial function also does not yield an improved empirical model (see SI-14). Both facts indicate that the presented empirical model provides the best description so far.

Although being frankly empirical, the obtained model is, to the best knowledge of the authors, the first model describing the friction behavior of chemically cross-linked hydrophilic lubricious coatings quantitatively. As indicated before, given the data,
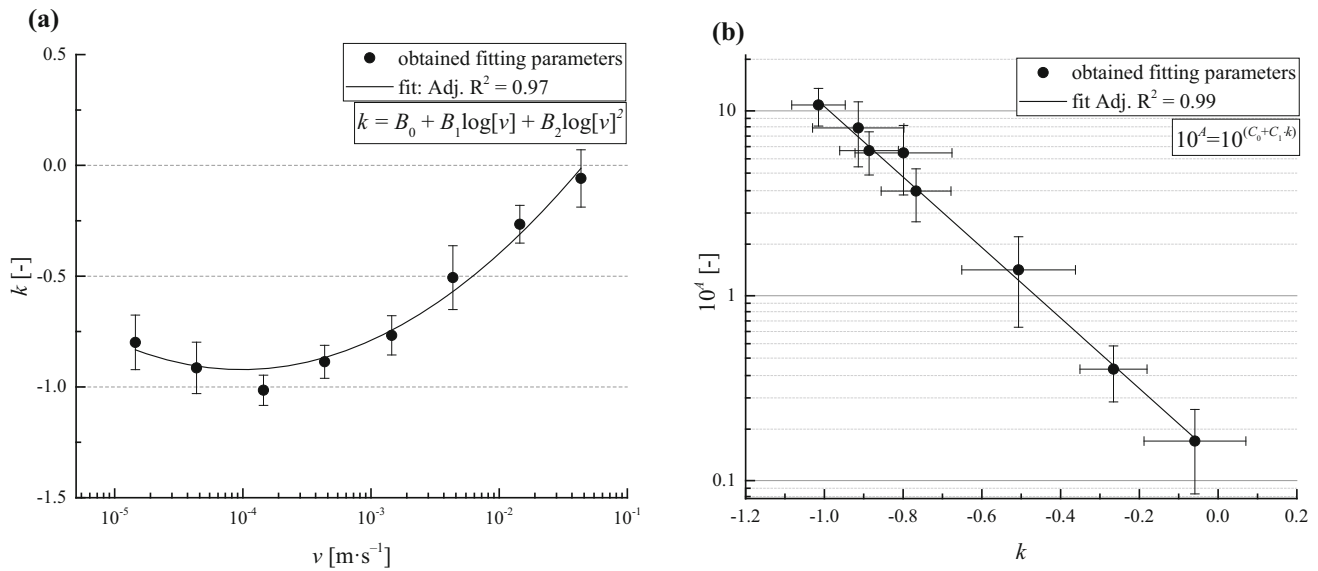
**Figure 8** **a** Plot of fitting parameter $k$ (from the slope of the fits of log[CoF] versus log[$\xi \cdot \varphi_{EG}$]) versus the sliding velocity $v$ and the associated parabolic fit. **b** Semi-log plot of $10^A$ versus $k$ and the associated linear fit. The error bars show the mean absolute deviation.
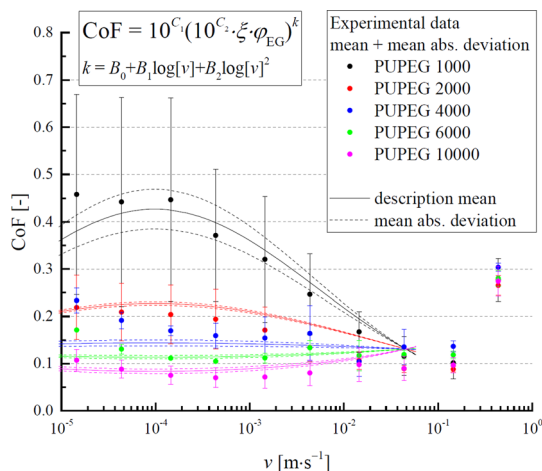


**Figure 9** Measured mean coefficient of friction (CoF) (symbols) versus the sliding velocity $v$ of the water-swollen PEG-based PU coatings with varying $M_n$ precursors, measured in demineralized water against a glass counter surface at a normal load of 0.5 N and empirical predictions (solid lines) based on the calculated mesh size $\xi$ from the obtained indentation modulus $E$. The error bars show the mean absolute deviation.

the shape of the $k$ versus log[$v$] curves seems to be symmetric. This symmetric shape of behavior versus log[$v$] is also seen in the adhesive friction and shear stress of rubbers [25, 65–67] as well as in the elastic adhesive friction dominated regime in the gel-friction mechanism [21, 24]. This indicates that information about the intrinsic polymer (structure) relaxation times and surface adsorption/desorption times is

included in the fitted parameters. Furthermore, it is expected that performing a similar study on well-defined polymer coatings prepared from different cross-linkers and/or polymer precursors will yield different values for the fitted parameters. In turn, these values could be correlated to yield a structure-parameter relation for a more generic empirical model for the structure–friction behavior relation of hydrophilic cross-linked polymer coatings in general.

## Conclusions

The coating network properties and aqueous friction behavior of swollen PEG-based PU network coatings with varying network precursor molar masses $M_n$ were studied. The water uptake and hydrophilicity of the surface increase upon increasing the $M_n$ of the precursor, whereas the indentation modulus of the swollen immersed coatings decreases, as expected. The molar mass between cross-links $M_c$ is calculated based on water uptake as well as on indentation data assuming an in-plane constrained swelling deformation, as expected for coatings with a very small aspect ratio adhering to a stiff (glass) substrate. These calculations are based on the phantom network model, taking into account network imperfections.

The friction behavior of the swollen coatings was measured using a custom-made immersed tribology setup, designed for measuring the macroscopic

aqueous friction response of swollen hydrophilic coatings against a glass counter surface when immersed in water. This tribometer is sensitive enough to measure significant differences in friction response for coatings prepared from precursor with different $M_n$ for a velocity range over 5 orders of magnitude. A clear transition is observed from the regime in which the indenter head contacts the coatings to the hydrodynamic lubrication regime where contact is lost. Moreover, as expected, a decrease in overall friction response upon increase of the network mesh size is observed in the interaction regime where the indenter actually makes contact.

The obtained friction, swelling and indentation data were used to successfully deduce an empirical model for the quantitative description of the friction behavior of the PEG-based PU coatings against a glass counter surface. This empirical model only depends on the mesh size of the coatings and the sliding velocity, thereby providing the first model of its kind for the description of the friction behavior of chemically cross-linked hydrophilic polymer coatings.

## Acknowledgements

**Electronic supplementary material:** The online version of this article (https://doi.org/10.1007/s108 53-020-05580-9) contains supplementary material, which is available to authorized users.

## References

[1] Wyman P (2012) Coatings for biomedical applications - chapter 1 hydrophilic coatings for biomedical applications in and ex vivo. Woodhead Publishing Limited, New Delhi

[2] Drelich J, Chibowski E, Meng DD, Terpilowski K (2011) Hydrophilic and superhydrophilic surfaces and materials. Soft Matter 7:9804–9828

[3] Chopra AM, Mehta M, Bismuth J, Shapiro M, Fishbein MC, Bridges AG, Vinters HV (2017) Polymer coating embolism from intravascular medical devices - a clinical literature review. Cardiovasc Pathol 30:45–54

[4] Dellimore KH, Helyer AR, Franklin SE (2013) A scoping review of important urinary catheter induced complications. J Mater Sci Mater Med 24:1825–1835

[5] Waller L, Jonsson O, Norlen L, Sullivan L (1995) Clean intermittent catheterization in spinal-cord injury patients - long-term follow-up of a hydrophilic low-friction technique. J Urol 153:345–348

[6] LaPorte RJ (1997) Hydrophilic polymer coatings for medical devices - structure/properties manufacture and applications development. CRC Press LLC, FL

[7] Slaughter BV, Khurshid SS, Fisher OZ, Khademhosseini A, Peppas NA (2009) Hydrogels in regenerative medicine. Adv Mater 21:3307–3329

[8] Peppas NA, Hilt JZ, Khademhosseini A, Langer R (2006) Hydrogels in biology and medicine: from molecular principles to bionanotechnology. Adv Mater 18:1345–1360

[9] Devine DM, Geever LM, Higginbotham CL (2005) Drug release from a N-vinylpyrrolidinone/acrylic acid lubricious hydrophilic coating. J Mater Sci 40:3429–3436. https://doi.org/10.1007/s10853-005-0416-2

[10] Telford AM, James M, Meagher L, Neto C (2010) Thermally cross-linked PNVP films as antifouling coatings for biomedical applications. ACS Appl Mater Interfaces 2:2399–2408

[11] Hanley P, Dolan F, Higginbotham C, and Tierney M (2007) "Coating for biomedical devices". USA Patent US2007043160A1, 2007

[12] Dias AJAA, Hensen GJE, Belt JW, Rooijmans M, Bond de NHM, and Currie EPK (2007) "Hydrophilic coating comprising a polyelectrolyte". WO Patent WO2007065722A1, 2007

[13] van Bochove B, Rongen JJ, Hannink G, van Tienen TG, Buma P, Grijpma DW (2015) Grafting a lubricious coating onto photo-crosslinked poly(trimethylene carbonate). Polym Adv Technol 26:1428–1432

[14] Militello M (2017) "Lubricious coating for medical device". WO Patent WO2017173114 (A1), 2017

[15] Elton RK (2011) "Hydrophilic coating composition comprising cross-linked polyurethane-based lubricious layers,". USA Patent US 20110144579A1, 2011

[16] Niemczyk A, El Fray M, Franklin SE (2015) Friction behavior of hydrophilic lubricious coatings for medical device applications. Tribol Int 89:54–61

[17] Bongaerts JHH, Cooper-White JJ, Stokes JR (2009) Low biofouling chitosan-hyaluronic acid multilayers with ultra-low friction coefficients. Biomacromol 10:1287–1294

[18] Ding X, Yang C, Lim TP, Hsu LY, Engler AC, Hedrick JL, Yang YY (2012) Antibacterial and antifouling catheter coatings using surface grafted PEG-b-cationic polycarbonate diblock copolymers. Biomaterials 33:6593–6603

[19] Kim BS, Hrkach JS, Langer R (2000) Biodegradable photo-crosslinked poly(ether-ester) networks for lubricious coatings. Biomaterials 21:259–265

[20] Nagaoka S, Akashi R (1990) Low-friction hydrophilic surface for medical devices. Biomaterials 11:419–424

[21] Gong JP (2006) Friction and lubrication of hydrogels—its richness and complexity. Soft Matter 2:544–552

[22] Spencer ND (2014) Aqueous lubrication - natural and biomimetic approaches. World Scientific Publishing Co Pvt Ltd, Singapore

[23] Kurokawa T, Tominaga T, Katsuyama Y, Kuwabara R, Furukawa H, Osada Y, Gong JP (2005) Elastic-hydrodynamic transition of gel friction. Langmuir 21:8643–8648

[24] Gong J, Osada Y (1998) Gel friction: a model based on surface repulsion and adsorption. J Chem Phys 109:8062–8068

[25] Schallamach A (1963) A theory of dynamic rubber friction. Wear 6:375–382

[26] de Gennes PG (1979) Scaling concepts in polymer physics. Cornell University Press, NY

[27] Gong JP, Iwasaki Y, Osada Y, Kurihara K, Hamai Y (1999) Friction of gels. 3. friction on solid surfaces. J Phys Chem B 103:6001–6006

[28] Tominaga T, Takedomi N, Biederman H, Furukawa H, Osada Y, Gong JP (2008) Effect of substrate adhesion and hydrophobicity on hydrogel friction. Soft Matter 4:1033–1040

[29] Tominaga T, Kurokawa T, Furukawa H, Osada Y, Gong JP (2008) Friction of a soft hydrogel on rough solid substrates. Soft Matter 4:1645–1652

[30] Kii A, Xu J, Gong JP, Osasa Y, Zhang XM (2001) Heterogeneous polymerization of hydrogels on hydrophobic substrate. J Phys Chem B 105:4565–4571

[31] Ohsedo Y, Takashina R, Gong JP, Osada Y (2004) Surface friction of hydrogels with well-defined polyelectrolyte brushes. Langmuir 20:6549–6555

[32] Du M, Zhang Y, Song Y, Zheng Q (2014) Negative velocity dependence of friction for poly(2-Acrylamido-2-methyl propanesulfonic acid) hydrogel sliding against a glass surface in the low-velocity region. J Polym Sci, Part B: Polym Phys 52:765–772

[33] Kozbial A, Li L (2014) Study on the friction of kappa-carrageenan hydrogels in air and aqueous environments. Mater Sci Eng C Mater Biol Appl 36:173–179

[34] Uruena JM, Pitenis AA, Nixon RM, Schulze KD, Angelini TE, Sawyer WG (2015) Mesh size control of polymer fluctuation lubrication in gemini hydrogels. Biotribology 1:24–29

[35] Pitenis AA, Uruena JM, Cooper AC, Angelini TE, Sawyer WG (2016) Superlubricity in gemini hydrogels. J Tribol-Trans Asme 138:7–9

[36] Dunn AC, Uruena JM, Huo YC, Perry SS, Angelini TE, Sawyer WG (2013) Lubricity of surface hydrogel layers. Tribol Lett 49:371–378

[37] Dunn AC, Sawyer WG, Angelini TE (2014) Gemini interfaces in aqueous lubrication with hydrogels. Tribol Lett 54:59–66

[38] Pitenis AA, Uruena JM, Schulze KD, Nixon RM, Dunn AC, Krick BA, Sawyer WG, Angelini TE (2014) Polymer fluctuation lubrication in hydrogel gemini interfaces. Soft Matter 10:8955–8962

[39] Rudin A (1999) The elements of polymer science and technology. Academic Press, Cambridge

[40] Hild G (1998) Model networks based on endlinking processes - synthesis structure and properties. Prog Polym Sci 23:1019–1149

[41] Gullapalli RP, Mazzitelli CL (2015) Polyethylene glycols in oral and parenteral formulations-a critical review. Int J Pharm 496:219–239

[42] "Molecular Modelling Pro," Version 6.3.3: Norgwyn Montgomery Software Inc., North Wales, PA, 1992

[43] Van Krevelen DW (1990) Properties of polymers. Elsevier, Amsterdam

[44] Hertz H (1882) Über die Berührung fester elastischer Körper. J reine und angewandte Mathematik 92:156–171

[45] Johnson KL (1985) Contact mechanics, 1st edn. Cambridge University Press, Cambridge

[46] Fishcher-Cripps AC (2004) Nanoindentation, 2nd edn. Springer Science+Business Media, Germany

[47] Canal T, Peppas NA (1989) Correlation between mesh size and equilibrium degree of swelling of polymeric networks. J Biomed Mater Res 23:1183–1193

[48] Mark JE, Flory PJ (1965) Configuration of polyoxyethylene chain. J American Chem Soc 87:1415

[49] Cruise GM, Scharp DS, Hubbell JA (1998) Characterization of permeability and network structure of interfacially photopolymerized poly(ethylene glycol) diacrylate hydrogels. Biomaterials 19:1287–1294

[50] Zustiak SP, Leach JB (2010) Hydrolytically degradable poly(ethylene glycol) hydrogel scaffolds with tunable degradation and mechanical properties. Biomacromol 11:1348–1357

[51] Erman B, Mark JE (1997) Structure and properties of rubberlike networks. Oxford University Press Inc, NY

[52] Flory PJ (1953) Principles of polymer chemistry. Cornell University Press, NY

[53] Horkay F, McKenna GB (2007) Polymer networks and gels. In: Mark JE (ed) Physical properties of polymers handbook,

2nd edn. Springer Science + Business Media, New York, pp 497–523

[54] Hild G (1997) Interpretation of equilibrium swelling data on model networks using affine and "phantom" network models. Polymer 38:3279–3293

[55] Saalwächter K, Chassé W, Sommer J-U (2013) Structure and swelling of polymer networks: insights from NMR. Soft Matter 9:6587

[56] Russ T, Brenn R, Geoghegan M (2003) Equilibrium swelling of polystyrene networks by linear polystyrene. Macromolecules 36:127–141

[57] Valentin JL, Carretero-Gonzalez J, Mora-Barrantes I, Chasse W, Saalwachter K (2008) Uncertainties in the determination of cross-link density by equilibrium swelling experiments in natural rubber. Macromolecules 41:4717–4729

[58] Erman B, Flory PJ (1982) Relationships between stress, strain, and molecular constitution of polymer networks - comparison of theory with experiments. Macromolecules 15:806–811

[59] Albers PTM, van der Ven LGJ, van Benthem RATM, Esteves ACC, de With G (2018) Water swelling behavior of poly(ethylene glycol)-based polyurethane networks. Macromolecules 53:862–874

[60] Miller DR, Macosko CW (1976) New derivation of post gel properties of network polymers. Macromolecules 9:206–211

[61] Miller DR, Valles EM, Macosko CW (1979) Calculation of molecular-parameters for stepwise polyfunctional polymerization. Polym Eng Sci 19:272–283

[62] Campise F, Agudelo DC, Acosta RH, Villar MA, Valles EM, Monti GA, Vega DA (2017) Contribution of entanglements to polymer network elasticity. Macromolecules 50:2964–2972

[63] Gnanou Y, Hild G, Rempp P (1987) Molecular structure and elastic behavior of PEG networks swollen to equilibrium. Macromolecules 20:1662–1671

[64] Hsu S, Ying C, Zhao F (2013) The nature of friction: a critical assessment. Friction 2:1–26

[65] Vorvolakos K, Chaudhury MK (2003) The effects of molecular weight and temperature on the kinetic friction of silicone rubbers. Langmuir 19:6778–6787

[66] Persson BNJ, Volokitin AI (2006) Rubber friction on smooth surfaces. European Phys J E 21:69–80

[67] Grosch KA (1963) "Relation between friction and viscoelastic properties of rubber," Proceedings of the royal society of London series a-mathematical and physical sciences 274, 21

**Publisher's Note** Springer Nature remains neutral with regard to jurisdictional claims in published maps and institutional affiliations.